Quantum Dot−DNA FRET Conjugates for Direct Analysis of Methylphosphonic Acid in Complex Media

Steven M. E. Demers,* Wendy W. Kuhne, Ashlee R. Swindle, Don D. Dick, and Kaitlin J. Coopersmith

ACCESS | Metrics & More | Article Recommendations | Supporting Information

ABSTRACT: Rapid detection of nerve agents from complex matrices with minimal sample preparation is essential due to their high toxicity and bioavailability. In this work, quantum dots (QDs) were functionalized with oligonucleotide aptamers that specifically targeted a nerve agent metabolite, methylphosphonic acid (MePA). These QD-DNA bioconjugates were covalently linked to quencher molecules to form Förster resonance energy transfer (FRET) donor−acceptor pairs that quantitatively measure the presence of MePA. Using the FRET biosensor, the MePA limit of detection was 743 nM in artificial urine. A decrease in the QD lifetime was measured upon DNA binding and was recovered with MePA. The biosensor's flexible design makes it a strong candidate for the rapid detection of chemical and biological agents for deployable, in-field detectors.
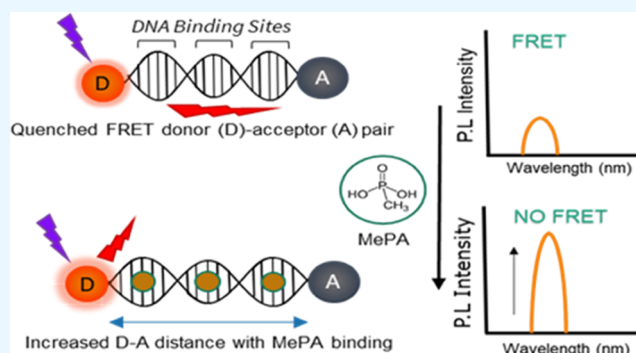
INTRODUCTION

Methylphosphonic acid (MePA) is a common human metabolite for phosphate-based chemical nerve agents and general insecticides and herbicides.[1−7] Chemical nerve agents remain a threat due to continued interest and use by military and terrorist organizations.[8] They often have low lethal dose (LD) thresholds, on the order of parts per million,[8] and the relative ease and variety of possible delivery methods make them particularly dangerous.[6] Additionally, there are many industrial uses for chemical nerve agents that prevent the prohibition of their manufacturing,[9] such as modern insecticides and herbicides.[10−13] MePA is an effective detection target for nerve agent exposure in human biological byproducts. The reported MePA median lethal dose is 2−135 μg/L, or about 20.8−960 nM.[3,14,15] Traditional analytical techniques either require complex and time-consuming processes or have detection limits (DLs) within or above the median lethal dose, limiting their utility for in-field detection. Overcoming the challenge of rapid and sensitive detection of chemical nerve agents and their metabolites in complex media is important for biological assays, environmental monitoring, and emergency response.

Currently, mass spectrometry (MS) and gas chromatography (GC) techniques are the most common methods for nerve agent confirmation.[2,5,15−21] MS methods are the most highly sensitive, with reported detection limits on the order of 10−50 nM (1−4 ng/mL).[2,17] While MS and GC methods are powerful and sensitive techniques, they require intricate and time-consuming sample preparation and analyses. The presence of interfering molecules has also been shown to be detrimental to detection limits. For example, GC detection limits for MePA in urine were reported to be 625 nM,[14] which is significantly higher than 30−100 nM for MePA detected in groundwater sources.[12] Detection of these metabolites in biological materials, such as blood or urine, below the median lethal dose requires additional sample processing.

For successful in-field detection, methods that require less power and simpler sample preparation techniques for MePA detection are desired. Raman and IR spectroscopy vibrational studies have been explored for rapid detection of MePA using simple sample preparation processing.[11,22,23] For example, surface-enhanced Raman spectroscopy (SERS) has been used to characterize the different vibrational modes of MePA and nerve agents in different environmental conditions.[22,23] However, vibrational spectroscopy techniques are often plagued by long integration times, which are exacerbated in complex media. For in-field detection, various colorimetric schemes utilized different binding and detection schemes but with limits of detection above the median lethal dose (LD50).[24−26]

In this work, a Förster resonance energy transfer (FRET)-based biosensor was created to overcome the shortfalls
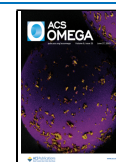
exhibited by these techniques. FRET-based detection methods are highly sensitive with minimal sample preparation and response times on the order of seconds to minutes. In FRET, an excited donor molecule transfers energy to an acceptor molecule through nonradiative dipole−dipole interactions.[27−34] For successful FRET, the donor and acceptor molecules need to have the appropriate spectral overlap, where the emission of the donor overlaps with the absorbance of the acceptor (overlap integral, J) and the donor (D) and acceptor (A) molecules should be in close proximity (1−10 nm separation). This short separation required for spectral overlap can be accomplished by covalently linking the donor and acceptor molecules. The transfer efficiency between a donor and acceptor is very sensitive and is proportional to $1/r^6$ (r = D−A distance). Upon analyte binding, a decrease in transfer efficiency occurs due to a change in the distance between the covalently bound donor and acceptor. This strong distance dependence leads to lower detection limits for FRET-based systems. This makes them ideal for in-field detection due to the lower detection limits, small sample size, and reduced power requirements.[26,35,36]

The use of targeting molecules, such as aptamers, can increase the specificity of these techniques. DNA aptamers have been developed that target MePA and other nerve agent derivatives, even in the presence of similar molecules.[37−40] The aptamer binding sites for MePA (TTTAGT) were identified using a combination of experiments and modeling.[37,38]

The goal of this work is to create a sensor that is highly sensitive to MePA to achieve a detection limit within or below the LD50 (20.8−960 nM) even in complex media without the need for further purification. Figure 1 shows the general sensor
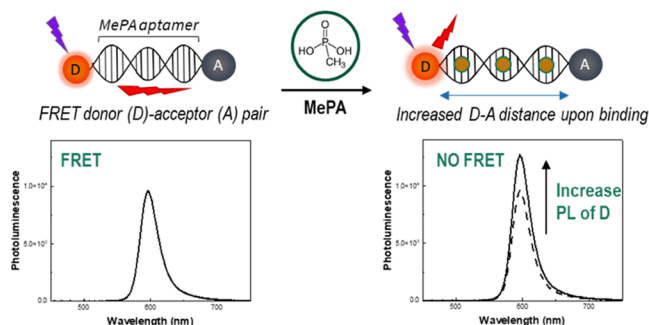

Figure 1. FRET-based biosensor composed of QD donor (D) and dye acceptor (A) bound together through a DNA aptamer. Each DNA aptamer has three binding sites for MePA. When MePA binds to the aptamer, a conformational change of the DNA between the donor and acceptor leads to a quantifiable change in the fluorescence (photoluminescence (PL)) signal.

design for MePA. Donor and acceptor molecules were functionalized with DNA aptamers that specifically targeted MePA through three TTTAGT binding sites. In the presence of MePA, the FRET between the donor and acceptor decreased due to the increased distance upon MePA binding, leading to a restoration of the fluorescence signal. Quantum dots were used as the fluorescence donor due to their high propensity for energy transfer,[41,42] tailorable optical and electronic properties,[43] and ability for surface functionalization.[44]

■ RESULTS AND DISCUSSION

QD-DNA conjugates were hybridized with Black Hole Quencher-2 functionalized complementary strands (BHQ) to create the FRET pair. QD-DNA−BHQ samples were then exposed to MePA to investigate the effect of analyte addition on the measured fluorescence signal between the QD donor and BHQ acceptor (Figure 2). Addition of MePA led to a
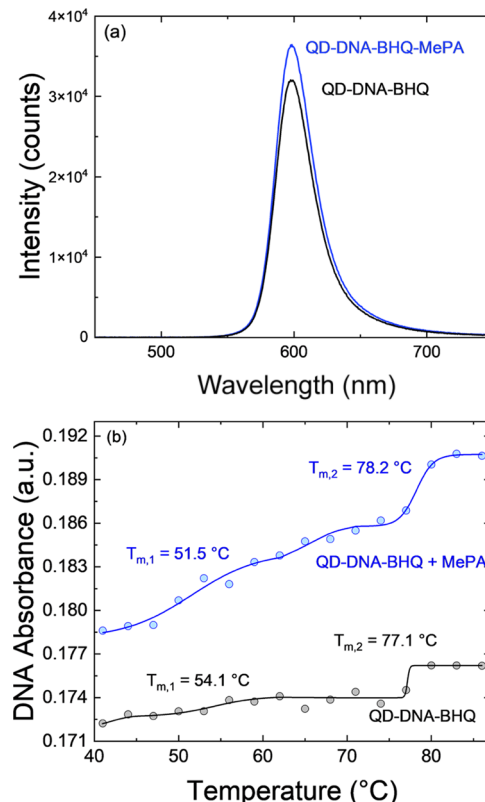

Figure 2. Effect of MePA addition on (a) fluorescence intensity and (b) DNA melting curves for QD-DNA−BHQ (T_{m1} = 54.1 °C; T_{m2} = 77.1 °C) and QD-DNA−BHQ-MePA (T_{m1} = 51.5 °C; T_{m2} = 78.2 °C). [MePA] = 208 nM. The melting curves are fit with Boltzmann fits to measure the T_m. The melting points were determined by examination of the second derivative of the DNA melting curves.

restoration of the FRET signal. This is attributed to a conformational change in the aptamer upon MePA addition due to an increase in the distance between the donor and
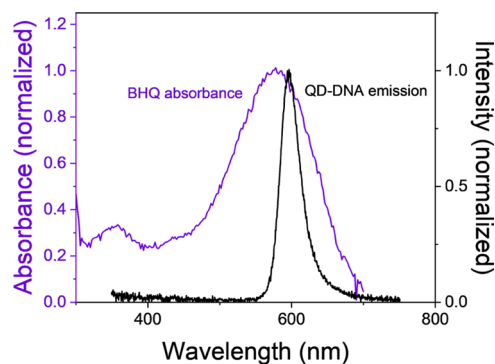

Figure 3. Spectral overlap between the emission of the QD donor and absorbance of the BHQ acceptor.

acceptor. A change in the DNA melting temperature was also measured after MePA addition, from 77.1 °C for QD-DNA−BHQ to 78.2 °C after MePA addition, as determined by the second derivative of the DNA melting curve. The slight increase in melting temperature is attributed to an increased rigidity in the DNA from MePA interaction or integration into the double-helix structure at the binding sites.[45] The spectral overlap between the QD emission and the BHQ is shown in Figure 3.

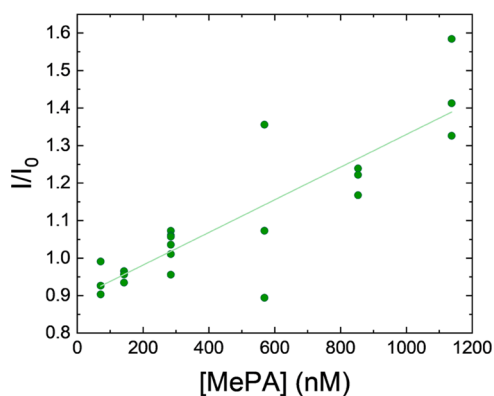A MePA calibration curve was created for urine-doped phosphate-buffered saline (PBS) (Figure 4) to test the

Figure 4. MePA calibration curve in artificial urine. Data collected from several measurements at each concentration. The detection limit was calculated from the linear range of the data depicted.

specificity of the FRET conjugates in a complex sample. Multiple trials were conducted at each MePA concentration across several days. At MePA concentrations above roughly 80 nM, an increase in fluorescence signal is observed due to an increase in donor−acceptor distance with the integration of MePA into the DNA strand, as depicted in Figure 1.

A detection limit of 743 nM was calculated using the residual sum of squares regression of the positively sloped linear region in Figure 4. The detection limit for MePA in artificial urine was comparable to those results using GC techniques in purified samples, though less than the results reported with MS. Reported detection limits using MS are around 10−50 nM (1−4 ng/mL) in buffer.[2,17] In artificial urine, the reported detection limit using GC was 625 nM.[14] Colorimetric techniques lead to detection limits on the order of hundreds of nanomolar.[26,35,36] Our reported FRET biosensor-measured detection limit was below the median lethal dose (<960 nM) in complex media without the need for further purification, demonstrating a robust, faster detection capability.

To verify that FRET signal response was due to nonradiative energy transfer between the donor and acceptor rather than the reverse, non-FRET-related quenching mechanisms, the fluorescence response with MePA in the absence of BHQ was measured, as shown in Figures 5 and 6.

The QD samples without bound amine DNA were exposed to MePA in PBS and urine and compared to QD-DNA without BHQ. For the samples without DNA, a decrease in I/I_0 after MePA addition is due to the quenching of the QDs after thorough binding between the mercaptopropionic ligands of the QD and the phosphate group of the MePA. In the absence of BHQ, quenching of the QD-DNA samples was not observed in the presence of MePA. Non-FRET-related quenching
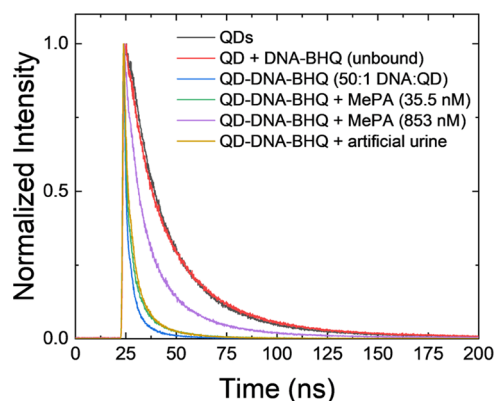

Figure 5. Lifetime measurements for different combinations of the biosensor components and analyte solution. Note that the "biosensor" solutions are the fully assembled DNA biosensors from conjugated QDs hybridized with DNA-quencher strands.
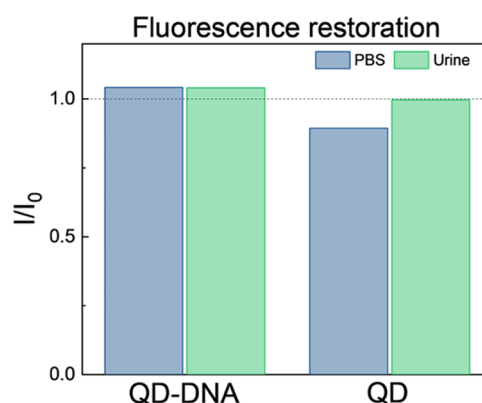

Figure 6. Change in fluorescence (I/I_0) for QD-DNA and QD without BHQ. MePA (208 nM) was added to each mixture. Note the decrease in fluorescence for those QDs coated with MPA compared to increased fluorescence of QD-DNA solutions.

mechanisms, such as MePA-induced precipitation or energy transfer to MePA, were not observed in the QD-DNA conjugates. This finding also shows the stability of the biosensor, where a positive identification signal can be observed even in the presence of potentially degrading matrix compounds.

Additionally, QD lifetimes were measured for QDs with and without DNA and MePA, as shown in Figure 5 and Table 1 using the same conditions as those for the calibration curve. The lifetime measurement fitting for each curve is shown in Figure S7.

As shown in Table 1, unbound QDs with BHQ did not change the QD lifetime, showing the binding was required for FRET to occur. After DNA conjugation, QD-DNA−BHQ had significantly shorter lifetimes, decreasing from 20.8 to 1.7 ns

Table 1. Lifetime Measurements

sample	measured lifetime (ns)
QD	20.8 ± 3.1
QD + DNA−BHQ (unbound)	20.4 ± 1.5
QD-DNA−BHQ (50:1 DNA/QD)	1.7 ± 0.5
QD-DNA−BHQ + MePA (35.5 nM)	2.8 ± 0.7
QD-DNA−BHQ + MePA (853 nM)	11.0 ± 1.3
QD-DNA−BHQ + artificial urine	3.2 ± 0.7

due to the energy transfer to the quencher. With the addition of MePA, the lifetime increased with concentration due to the increased distance after the MePA bound to the DNA aptamer, causing the strand to expand. The increase in QD lifetimes with the addition of MePA is evidence that the detection is occurring due to energy transfer between the QD donors and quencher acceptors.

In summary, this initial investigation into using a FRET-based biosensor was successful in the detection of methyl-phosphonic acid in complex matrices without the need for further purification. To increase the viability for in-field detection, future work will focus on testing the biosensor with other similar analytes and with random DNA strands to test the specificity of this design.[37,38] Subsequent investigations using this biosensor design will investigate the effect of QD-gold nanoparticle energy transfer pairs to increase the sensitivity of this technique through nanometal surface energy transfer (NSET). The DNA strand length and sequence can also be tailored for the modular detection of different analytes. A different QD-DNA conjugation technique can also be utilized to decrease detection limits, such as by Green et al. for closer QD-BHQ distances and thus a greater FRET response and higher analyte sensitivity.[46,47]

CONCLUSIONS

The ability to detect the nerve agent metabolite methyl-phosphonic acid (MePA) in complex media without the need for further purification has been demonstrated. QD-DNA conjugates were coupled to a complementary strand that was functionalized with a FRET acceptor. DNA strands were designed to specifically target MePA at three binding sites between each QD-acceptor pairing. The calculated detection limit for MePA in artificial urine was 743 nM, showing this technique is sensitive even in complex matrices. The detection limit is comparable to other techniques such as MS and GCMS and is below the MePA median lethal dose (960 nM). The rapid response of fluorescence compared to MS and GC methods makes this a practical method for in-field detection of nerve agents and their metabolites. This work successfully demonstrates the ability of FRET-based biosensors to be utilized as on-site detection devices for chemical threats. Coupled with the ease of sample preparation for the biosensor solution, the FRET biosensor presented in this work is an appealing method for nerve agent metabolite detection.

EXPERIMENTAL SECTION

Chemicals. Organic-coated CdSe/ZnS quantum dots with a fluorescence peak at 600 nm were purchased from Ocean NanoTech (San Diego, CA). Modified oligonucleotides were obtained from Integrated DNA Technologies, Inc. (Coralville, IA) as lyophilized powders and dissolved in phosphate buffer. Artificial urine was purchased from Pickering Laboratories (Mountain View, CA). 2-Methylphosphonic acid (MPA), tetramethylammonium hydroxide (TMAH), chloroform, N-ethyl-N'-(3-dimethylaminopropyl)-carbodiimide hydrochloride (EDC), N-hydroxysulfosuccinimide sodium salt (NHS), sodium chloride (NaCl), monobasic and dibasic sodium phosphate, and borate buffer were purchased from Sigma-Aldrich (St. Louis, MO) and used without further purification. Phosphate buffer (PB) was created from monobasic and dibasic sodium phosphate. Phosphate-buffered saline (PBS) was made by dissolving 0.1 M NaCl in 0.01 M PB.

Quantum Dot Bioconjugation. Hydrophilic QDs with carboxyl functionalization were prepared via ligand exchange using 2-methylpropionic acid (MPA).[44] The bottom organic layer from a mixture of 500 μL of MPA with 1 g of TMAH in 10 mL of $CHCl_3$ was added to 1 mL of QDs dispersed in $CHCl_3$. This mixture was maintained at ambient room temperature until the hydrophilic QDs formed a top layer of QD-MPA. The top layer was removed, and the QDs were washed with fresh $CHCl_3$ and precipitated in methanol. The methanol supernatant was removed, and the cleaned QDs were dispersed in borate buffer. Amine-modified DNA (5′-AAC CGG CGT TTA GTG CCT TTA GTC GGT TTA GTG CCT ACC G-PEG9spacer (amino)-3′) was conjugated to QDs using EDC/NHS coupling[48] to create QD-DNA conjugates. The three anticipated MePA binding sites are underlined for the DNA aptamer. To remove excess DNA, the conjugated QDs were purified using a 50 kDa Amicon spin filter (Sigma-Aldrich; St. Louis, MO) and resuspended in fresh borate buffer (1 M borate buffer, 0.1 M NaCl). The final QD-DNA conjugates had a quantum yield of ~12%.

DNA Quantification. The effective ratio of DNA loading was measured using UV−vis spectroscopy. First, QD-DNA conjugates were incubated with complementary strands at room temperature. After 1 h, the QDs were centrifuged for 1 h at 10k rpm at 20 °C using a 50 kDa Amicon spin filter (Sigma-Aldrich; St. Louis, MO) to separate the QDs from the unbound complementary strand. The filtrate was removed, and the concentration of the unbound DNA in the filtrate was compared to control complementary strands without QDs using UV−vis spectroscopy.

Characterization. UV−vis and fluorescence measurements were collected on a Horiba Duetta spectrometer (Horiba; Irvine CA). UV−vis measurements were obtained with 5 nm bandpass and 0.05 s integration. UV−vis DNA melting curves were measured in the UV−vis at T = 20−95 °C in 3 °C step increments with 5-min equilibrium time between each measurement. Fluorescence measurements of QDs were carried out with an excitation wavelength of 300 nm with 5 nm emission and excitation slits. An average of 10 accumulations with 0.1 s integration time was measured for each sample. The relative quantum yield of the quantum dots was compared to rhodamine 6G (QY = 95%) reference dye. QD concentration was calculated from the QD extinction coefficient at the first excitonic absorption peak.[49] Measurements were taken with QD concentrations within the linear range of the fluorescence detector (Figure S1) to ensure a linear response with changes in the FRET signal.

FRET Measurements. FRET conjugates were prepared by mixing QD-DNA conjugates to their complementary strand. The DNA-quencher/QD ratio was held at 50:1 to ensure maximum QD quenching (Figure S2). Note that only ~20 DNA strands could be bound to each QD's surface during the conjugation process.[48] An excess of conjugate DNA strands was added to facilitate full hybridization of the DNA strands. The unbound DNA-quencher strands were found to have a negligible effect on the QDs emission, as seen in Figure 5.

The complementary strand was modified with Black Hole Quencher-2 as the FRET donor (BHQ = 5′-CGG TAG GCA CTA AAC CGA CTA AAG GCA CTA AAC GCC GGT T (BHQ-2)-3′) to create the FRET conjugate, QD-DNA−BHQ. The FRET conjugates' absorbances were examined at each step and can be seen in Section S5.

To create the MePA calibration curve, different concentrations of MePA were mixed with QD-DNA and shaken for 1 h to facilitate the complete binding of MePA to the DNA aptamer. These measurements were carried out in a PBS/urine mixture (50 μL of artificial urine in 600 μL of PBS).

Lifetime Measurements. Time-correlated single-photon counting was conducted on a FluoroMax Plus spectrofluorometer (Horiba; Irvine CA) equipped with a DeltaDiode Laser (DD-375L; Horiba) at 371 nm center wavelength using DeltaTime TCSPC. At least 10,000 counts were recorded for all lifetime measurements measured at the maximum fluorescence wavelength of roughly 590 nm. The samples were allowed to incubate for several weeks at 20 °C before they were measured.

Limit of Detection Calculations. The calibration curve was constructed for the FRET conjugates with MePA by plotting FRET response vs [MePA]. The data was brought into OriginPlot, and a linear fit was applied to all of the data points, using the regular residual analysis. The standard regression of the sum of squares method is given by the formula

$$\sigma = \frac{\text{residual sum of squares}}{\text{degrees of freedom}} \qquad (1)$$

The detection limit (DL) was calculated from σ of eq 1, and m is the slope of the best-fit line

$$DL = 3.3 \times \sigma/m \qquad (2)$$

FRET response was measured by comparing the signal of QD-DNA−BHQ in the absence (I_0) and presence (I) of MePA, normalized to the QD concentration by dividing QD peak emission by the QD absorbance at 400 nm to avoid interferences with the absorbance of urine (Figure S3). The peaks below 300 nm are due to the presence of chemicals found in artificial urine;[50] for example, uric acid has a high absorbance cross section around 295 nm.[51]

■ ASSOCIATED CONTENT

Ⓢ Supporting Information

The Supporting Information is available free of charge at https://pubs.acs.org/doi/10.1021/acsomega.3c02173.

> DNA strands used, linearity of fluorescence response as a function of QD concentration in buffer and PBS/urine, optimization of QD/BHQ ratio for maximum quenching in the system, quality control for assembly of biosensor components, initial testing of MePA binding to DNA binding sites, analysis decisions for normalization across different sample responses, individual lifetime measurements and fit values, and donor−acceptor FRET pairing calculations (PDF)

■ AUTHOR INFORMATION

Corresponding Author

Steven M. E. Demers − *Global Security Directorate, Savannah River National Laboratory, Aiken, South Carolina 29808, United States;* ⓘ orcid.org/0000-0001-9221-3246; Email: steven.demers@srnl.doe.gov

Authors

Wendy W. Kuhne − *Global Security Directorate, Savannah River National Laboratory, Aiken, South Carolina 29808, United States*

Ashlee R. Swindle − *Global Security Directorate, Savannah River National Laboratory, Aiken, South Carolina 29808, United States*

Don D. Dick − *Global Security Directorate, Savannah River National Laboratory, Aiken, South Carolina 29808, United States*

Kaitlin J. Coopersmith − *Global Security Directorate, Savannah River National Laboratory, Aiken, South Carolina 29808, United States;* Present Address: Entegris, Inc., 7 Commerce Road, Danbury, Connecticut 06810, United States; ⓘ orcid.org/0000-0001-6589-8825

Complete contact information is available at: https://pubs.acs.org/10.1021/acsomega.3c02173

Author Contributions

W.W.K., A.R.S., and K.J.C. designed the study. S.M.E.D., D.D.D., and K.J.C. prepared and performed the experiments and data analysis. S.M.E.D., K.J.C., W.W.K., and A.R.S. wrote and prepared the manuscript. All authors provided critical feedback.

Notes

The authors have filed provisional patent application US: 63/297,361: Biosensor for Simultaneous Chemical, Biological, and Radiological/Nuclear Detection to Battelle Savannah River Alliance, LLC.

The authors declare the following competing financial interest(s): The authors have filed provisional patent application US: 63/297,361: Biosensor for Simultaneous Chemical, Biological, and Radiological/Nuclear Detection to Battelle Savannah River Alliance, LLC.

This work was produced by Battelle Savannah River Alliance, LLC under Contract No. 89303321CEM000080 with the U.S. Department of Energy. Publisher acknowledges the U.S. Government license to provide public access under the DOE Public Access Plan (http://energy.gov/downloads/doe-public-access-plan).

■ ACKNOWLEDGMENTS

■ ABBREVIATIONS

MePA, methylphosphonic acid; QD, quantum dots; FRET, Förster resonance energy transfer; MS, mass spectroscopy; GC, gas chromatography; PBS, phosphate-buffered saline; BHQ, Black Hole Quencher-2 functionalized complementary DNA strands

■ REFERENCES

(1) Ashley, J. A.; Lin, C. H.; Wirsching, P.; Janda, K. D. Monitoring chemical warfare agents: A new method for the detection of methylphosphonic acid. *Angew. Chem., Int. Ed.* **1999**, *38*, 1793−1795.

(2) Baygildiev, T.; Zatirakha, A.; Rodin, I.; Braun, A.; Stavrianidi, A.; Koryagina, N.; Rybalchenko, I.; Shpigun, O. Rapid IC-MS/MS determination of methylphosphonic acid in urine of rats exposed to organophosphorus nerve agents. *J. Chromatogr. B: Anal. Technol. Biomed. Life Sci.* **2017**, *1058*, 32−39.

(3) Boland, D. M. Disposition of Toxic Drugs and Chemicals in Man, 12th Edition. *J. Anal. Toxicol.* **2021**, *44*, e13.

(4) Heleg-Shabtai, V.; Gratziany, N.; Liron, Z. Separation and detection of VX and its methylphosphonic acid degradation products on a microchip using indirect laser-induced fluorescence. *Electrophoresis* **2006**, *27*, 1996−2001.

(5) Lin, Y.; Chen, J.; Yan, L.; Guo, L.; Wu, B.; Li, C.; Feng, J.; Liu, Q.; Xie, J. Determination of nerve agent metabolites in human urine by isotope-dilution gas chromatography-tandem mass spectrometry after solid phase supported derivatization. *Anal. Bioanal. Chem.* **2014**, *406*, 5213−5220.

(6) Lukey, B. J.; Romano, J. A.; Harry, S. *Chemical Warfare Agents: Biomedical and Psychological Effects, Medical Countermeasures, and Emergency Response*, 3rd ed.; CRC Press, 2019.

(7) Thomson, S. *Analysis of Urinary Metabolites of Nerve and Blister Chemical Warfare Agents*; Defense Science and Technology Organization—Land Division, Defense Technical Information Center, 2014.

(8) Stuart, J. A.; Ursano, R. J.; Fullerton, C. S.; Norwood, A. E.; Murray, K. Belief in exposure to terrorist agents: Reported exposure to nerve or mustard gas by Gulf War veterans. *J. Nerv. Ment. Dis.* **2003**, *191*, 431−436.

(9) Chauhan, S.; Chauhan, S.; D'Cruz, R.; Faruqi, S.; Singh, K. K.; Varma, S.; Singh, M.; Karthik, V. Chemical warfare agents. *Environ. Toxicol. Pharmacol.* **2008**, *26*, 113−122.

(10) Getnet, D.; Gautam, A.; Kumar, R.; Hoke, A.; Cheema, A. K.; Rossetti, F.; Schultz, C. R.; Hammamieh, R.; Lumley, L. A.; Jett, M. Poisoning with Soman, an Organophosphorus Nerve Agent, Alters Fecal Bacterial Biota and Urine Metabolites: a Case for Novel Signatures for Asymptomatic Nerve Agent Exposure. *Appl. Environ. Microbiol.* **2018**, *84*, No. e00978-18.

(11) Myers, T. L.; Saunders, D. L.; Szecsody, J. E.; Tonkyn, R. G.; Mo, K. F.; Cappello, B. F.; Banach, C. A.; Fraga, C. G.; Johnson, T. J. Hydrolysis of methylphosphonic anhydride solid to methylphosphonic acid probed by Raman and infrared reflectance spectroscopies. *Anal. Methods* **2021**, *13*, 3863−3873.

(12) Sega, G. A.; Tomkins, B. A.; Griest, W. H. Analysis of methylphosphonic acid, ethyl methylphosphonic acid and isopropyl methylphosphonic acid at low microgram per liter levels in groundwater. *J. Chromatogr. A* **1997**, *790*, 143−152.

(13) Baygildiev, T. M.; Rodin, I. A.; Stavrianidi, A. N.; Braun, A. V.; Lebedev, A. T.; Rybalchenko, I. V.; Shpigun, O. A. Hydrophilic interaction liquid chromatography-tandem mass spectrometry methylphospnonic and alkyl methylphosphonic acids determination in environmental samples after pre-column derivatization with p-bromophenacyl bromide. *J. Chromatogr. A* **2016**, *1442*, 19−25.

(14) Minami, M.; Hui, D. M.; Katsumata, M.; Inagaki, H.; Boulet, C. A. Method for the analysis of the methylphosphonic acid metabolites of sarin and its ethanol-substituted analogue in urine as applied to the victims of the Tokyo sarin disaster. *J. Chromatogr. B: Biomed. Sci. Appl.* **1997**, *695*, 237−244.

(15) Noort, D.; Hulst, A. G.; Platenburg, D. H. J. M.; Polhuijs, M.; Benschop, H. P. Quantitative analysis of O-isopropyl methylphosphonic acid in serum samples of Japanese citizens allegedly exposed to sarin: estimation of internal dosage. *Arch. Toxicol.* **1998**, *72*, 671−675.

(16) B'Hymer, C. A Brief Overview of HPLC-MS Analysis of Alkyl Methylphosphonic Acid Degradation Products of Nerve Agents. *J. Chromatogr. Sci.* **2019**, *57*, 606−617.

(17) Li, B. Q.; Wei, J. N.; Kong, J. L.; Qin, M. L.; Yang, L.; Li, C. P. Rapid detection of Sarin hydrolysis products based on micro-extraction by packed sorbent combined with Nano-ESI mass spectrometry. *Int. J. Mass Spectrom.* **2021**, *461*, No. 116513.

(18) Rohrbaugh, D. K.; Sarver, E. W. Detection of alkyl methylphosphonic acids in complex matrices by gas chromatog-raphy−tandem mass spectrometry. *J. Chromatogr. A* **1998**, *809*, 141−150.

(19) Valdez, C. A.; Marchioretto, M. K.; Leif, R. N.; Hok, S. Efficient derivatization of methylphosphonic and aminoethylsulfonic acids related to nerve agents simultaneously in soils using trimethyloxonium tetrafluoroborate for their enhanced, qualitative detection and identification by EI-GC-MS and GC-FPD. *Forensic Sci. Int.* **2018**, *288*, 159−168.

(20) Yashin, Y. S.; Revelsky, I. A.; Tikhonova, I. N.; Karavaeva, V. G.; Virus, E. D.; Chepelyansky, D. A.; Revelsky, A. I. A Comparison of the Limits of Detection for a Number of Surrogates of Organophosphorus Toxic Agents and Methylphosphonic Acid Silyl Derivatives and its O-Alkyl Esters by Gas Chromatography/Mass Spectrometry with Various Ionization Methods and a Flameless Thermionic Ionization Detector. *J. Anal. Chem.* **2020**, *75*, 1653−1659.

(21) Kataoka, M.; Seto, Y. Discriminative determination of alkyl methylphosphonates and methylphosphonate in blood plasma and urine by gas chromatography-mass spectrometry after tert.-butyldimethylsilylation. *J. Chromatogr. B* **2003**, *795*, 123−132.

(22) Farquharson, S.; Gift, A.; Maksymiuk, P.; Inscore, F. Surface-Enhanced Raman Spectra of VX and its Hydrolysis Products. *Appl. Spectrosc.* **2005**, *59*, 654−660.

(23) Farquharson, S.; Gift, A.; Maksymiuk, P.; Inscore, F.; Smith, W. In *pH Dependence of Methyl Phosphonic Acid, Dipicolinic Acid, and Cyanide by Surface-Enhanced Raman Spectroscopy*, Proceedings of the Chemical and Biological Point Sensors for Homeland Defense; SPIE, 2004.

(24) Yao, J.; Zhang, K.; Zhu, H.; Ma, F.; Sun, M.; Yu, H.; Sun, J.; Wang, S. Efficient Ratiometric Fluorescence Probe Based on Dual-Emission Quantum Dots Hybrid for On-Site Determination of Copper Ions. *Anal. Chem.* **2013**, *85*, 6461−6468.

(25) Huy, G. D.; Zhang, M.; Zuo, P.; Ye, B.-C. Multiplexed analysis of silver(i) and mercury(ii) ions using oligonucletide−metal nanoparticle conjugates. *Analyst* **2011**, *136*, 3289−3294.

(26) Paterson, S.; de la Rica, R. Solution-based nanosensors for in-field detection with the naked eye. *Analyst* **2015**, *140*, 3308−3317.

(27) Breshike, C. J.; Riskowski, R. A.; Strouse, G. F. Leaving Förster Resonance Energy Transfer Behind: Nanometal Surface Energy Transfer Predicts the Size-Enhanced Energy Coupling between a Metal Nanoparticle and an Emitting Dipole. *J. Phys. Chem. C* **2013**, *117*, 23942−23949.

(28) Coopersmith, K.; Han, H.; Maye, M. M. Stepwise Assembly and Characterization of DNA Linked Two-Color Quantum Dot Clusters. *Langmuir* **2015**, *31*, 7463−7471.

(29) Singh, M. P.; Strouse, G. F. Involvement of the LSPR Spectral Overlap for Energy Transfer between a Dye and Au Nanoparticle. *J. Am. Chem. Soc.* **2010**, *132*, 9383−9391.

(30) Beljonne, D.; Curutchet, C.; Scholes, G. D.; Silbey, R. J. Beyond Forster Resonance Energy Transfer in Biological and Nanoscale Systems. *J. Phys. Chem. B* **2009**, *113*, 6583−6599.

(31) Berney, C.; Danuser, G. FRET or no FRET: A quantitative comparison. *Biophys. J.* **2003**, *84*, 3992−4010.

(32) Chen, G. W.; Song, F. L.; Xiong, X. Q.; Peng, X. J. Fluorescent Nanosensors Based on Fluorescence Resonance Energy Transfer (FRET). *Ind. Eng. Chem. Res.* **2013**, *52*, 11228−11245.

(33) Halivni, S.; Sitt, A.; Hadar, I.; Banin, U. Effect of Nanoparticle Dimensionality on Fluorescence Resonance Energy Transfer in Nanoparticle-Dye Conjugated Systems. *ACS Nano* **2012**, *6*, 2758−2765.

(34) Han, H.; Di Francesco, G.; Maye, M. M. Size Control and Photophysical Properties of Quantum Dots Prepared via a Novel Tunable Hydrothermal Route. *J. Phys. Chem. C* **2010**, *114*, 19270−19277.

(35) Huy, G. D.; Zhang, M.; Zuo, P.; Ye, B. C. Multiplexed analysis of silver(I) and mercury(II) ions using oligonucletide-metal nanoparticle conjugates. *Analyst* **2011**, *136*, 3289−3294.

(36) Yao, J. L.; Zhang, K.; Zhu, H. J.; Ma, F.; Sun, M. T.; Yu, H.; Sun, J.; Wang, S. H. Efficient Ratiometric Fluorescence Probe Based

on Dual-Emission Quantum Dots Hybrid for On-Site Determination of Copper Ions. *Anal. Chem.* **2013**, *85*, 6461−6468.

(37) Bruno, J. G.; Carrillo, M. P.; Cadieux, C. L.; Lenz, D. E.; Cerasoli, D. M.; Phillips, T. DNA aptamers developed against a soman derivative cross-react with the methylphosphonic acid core but not with flanking hydrophobic groups. *J. Mol. Recognit.* **2009**, *22*, 197−204.

(38) Bruno, J. G.; Carrillo, M. P.; Phillips, T.; Vail, N. K.; Hanson, D. Competitive FRET-aptamer-based detection of methylphosphonic acid, a common nerve agent metabolite. *J. Fluoresc.* **2008**, *18*, 867−876.

(39) Zhao, R.; Jia, D. L.; Wen, Y. Z.; Yu, X. M. Cantilever-based aptasensor for trace level detection of nerve agent simulant in aqueous matrices. *Sens. Actuators, B* **2017**, *238*, 1231−1239.

(40) Liu, Z. W.; Tong, Z. Y.; Hao, L. Q.; Liu, B.; Mu, X. H.; Zhang, J. P.; Gao, C. Aptamer-Based Microcantilever Sensor for O-ethyl S-[2(diisopropylamino)ethyl] methylphosphonothiolate, Sarin Detection and Kinetic Analysis. *Chin. J. Anal. Chem.* **2014**, *42*, 1143−1148.

(41) Cardoso Dos Santos, M.; Algar, W. R.; Medintz, I. L.; Hildebrandt, N. Quantum dots for Förster Resonance Energy Transfer (FRET). *TrAC, Trends Anal. Chem.* **2020**, *125*, No. 115819.

(42) Chou, K. F.; Dennis, A. M. Forster Resonance Energy Transfer between Quantum Dot Donors and Quantum Dot Acceptors. *Sensors* **2015**, *15*, 13288−13325.

(43) Aubert, T.; Golovatenko, A. A.; Samoli, M.; Lermusiaux, L.; Zinn, T.; Abecassis, B.; Rodina, A. V.; Hens, Z. General Expression for the Size-Dependent Optical Properties of Quantum Dots. *Nano Lett.* **2022**, *22*, 1778−1785.

(44) Banerjee, A.; Pons, T.; Lequeux, N.; Dubertret, B. Quantum dots-DNA bioconjugates: synthesis to applications. *Interface Focus* **2016**, *6*, No. 20160064.

(45) Liu, H. H.; Gao, Y. Q.; Mathivanan, J.; Shen, F. S.; Chen, X.; Li, Y. Y.; Shao, Z. W.; Zhang, Y. X.; Shao, Q. Y.; Sheng, J.; Gan, J. H. Structure-guided development of Pb2+-binding DNA aptamers. *Sci. Rep.* **2022**, *12*, No. 460.

(46) Green, C. M.; Hastman, D. A.; Mathur, D.; Susumu, K.; Oh, E.; Medintz, I. L.; Díaz, S. A. Direct and Efficient Conjugation of Quantum Dots to DNA Nanostructures with Peptide-PNA. *ACS Nano* **2021**, *15*, 9101−9110.

(47) Green, C. M.; Spangler, J.; Susumu, K.; Stenger, D. A.; Medintz, I. L.; Díaz, S. A. Quantum Dot-Based Molecular Beacons for Quantitative Detection of Nucleic Acids with CRISPR/Cas(N) Nucleases. *ACS Nano* **2022**, *16*, 20693−20704.

(48) Sun, D.; Gang, O. DNA-Functionalized Quantum Dots: Fabrication, Structural, and Physicochemical Properties. *Langmuir* **2013**, *29*, 7038−7046.

(49) Yu, W. W.; Qu, L. H.; Guo, W. Z.; Peng, X. G. Experimental determination of the extinction coefficient of CdTe, CdSe, and CdS nanocrystals. *Chem. Mater.* **2003**, *15*, 2854−2860.

(50) Sarigul, N.; Korkmaz, F.; Kurultak, I.; New, A. Artificial Urine Protocol to Better Imitate Human Urine. *Sci. Rep.* **2019**, *9*, No. 20159.

(51) Norazmi, N.; Abdul Rasad, Z. R.; Mohamad, M.; Manap, H. Uric acid detection using UV−vis spectrometer. *IOP Conf. Ser.: Mater. Sci. Eng.* **2017**, *257*, No. 012031.